Redox Biology (2016) 178–187

Contents lists available at ScienceDirect

Redox Biology

journal homepage: www.elsevier.com/locate/redox

Research paper

Uncoupling protein 2 modulation of the NLRP3 inflammasome in astrocytes and its implications in depression

Ren-Hong Du [a,1], Fang-Fang Wu [a,1], Ming Lu [a,1], Xiao-dong Shu [a], Jian-Hua Ding [a], Guangyu Wu [b], Gang Hu [a,c,*]

[a] Jiangsu Key Laboratory of Neurogeneration, Department of Pharmacology, Nanjing Medical University, 101 Nongmian Road, Nanjing, Jiangsu 210029, PR China
[b] Department of Pharmacology and Toxicology, Medical College of Georgia, Georgia Regents, 1459 Laney Walker Blvd., Augusta, GA 30912, United States
[c] Department of Pharmacology, Nanjing University of Chinese Medicine, 138 Xianlin Avenue, Nanjing, Jiangsu 210023, PR China

ARTICLE INFO

Article history:
Received 9 August 2016
Received in revised form
16 August 2016
Accepted 17 August 2016
Available online 18 August 2016

Keywords:
Uncoupling protein 2
NLRP3 inflammasome
Astrocyte
Depression
Reactive oxygen species

ABSTRACT

Mitochondrial uncoupling protein 2 (UCP2) has been well characterized to control the production of reactive oxygen species (ROS) and astrocytes are the major cells responsible for the ROS production and the inflammatory responses in the brain. However, the function of UCP2 in astrocytes and the contribution of astrocytic UCP2 to depression remain undefined. Herein, we demonstrated that UCP2 knockout (KO) mice displayed aggravated depressive-like behaviors, impaired neurogenesis, and enhanced loss of astrocytes in the chronic mild stress (CMS)-induced anhedonia model of depression. We further found that UCP2 ablation significantly enhanced the activation of the nod-like receptor protein 3 (NLRP3) inflammasome in the hippocampus and in astrocytes. Furthermore, UCP2 deficiency promoted the injury of mitochondria, the generation of ROS and the physical association between thioredoxin-interacting protein (TXNIP) and NLRP3 in astrocytes. Moreover, transiently expressing exogenous UCP2 partially rescued the deleterious effects of UCP2 ablation on the astrocytes. These data indicate that UCP2 negatively regulates the activation of NLRP3 inflammasome and inhibited the ROS-TXNIP-NLRP3 pathway in astrocytes. Collectively, our findings reveal that UCP2 regulates inflammation responses in astrocytes and plays an important role in the pathogenesis of depression and that UCP2 may be a promising therapeutic target for depression.

1. Introduction

Major depressive disorder (MDD) is a major cause of disability that affects approximately 16% of the world's population [1] and has been characterized to associate with activated oxidative stress [2], mitochondrial dysfunction [3], reduced neurogenesis [4] and chronic inflammation [5]. In the brain, astrocytes, the most numerous and versatile of all types of glial cells, are responsible for the production of reactive oxygen species (ROS) and pro-inflammatory cytokines, such as interleukin (IL)-1β that has been demonstrated to be a crucial factor in the induction of depressive symptomatology [6,7]. First, the expression level of IL-1β is consistently increased in the blood or the brain of the depressed patients, which is clearly correlated with the severity of disease [8]. Second, administration of exogenous IL-1β, either peripherally or directly into the brain, produces depressive-like symptoms [9,10], whereas blockade of the IL-1 receptor inhibits these stress-like effects [11]. Third, antidepressant treatment can attenuate depressive-like behavior through inhibiting the function of IL-1β [12].

IL-1β production is tightly controlled by inflammasome, an intracellular multiprotein complex that consists of nod-like receptor protein (NLRP), adaptor protein ASC and procaspase-1 [13]. Among the NLR family, the NLRP3 inflammasome is the most extensively studied and best understood member [14]. It is well known that NLRP3 inflammasome can be activated by a variety of danger signals, such as pathogen-associated molecular patterns [15] and danger-associated molecular patterns [16] and the production of ROS has been demonstrated to act as a common cellular signal upstream of NLRP3 activation [17]. ROS promotes the dissociation of thioredoxin-interacting protein (TXNIP) from thioredoxin and allows TXNIP to bind to NLRP3, and subsequently

* Corresponding author at: Jiangsu Key Laboratory of Neurogeneration, Department of Pharmacology, Nanjing Medical University, Nanjing, Jiangsu 210029, PR China.
E-mail address: ghu@njmu.edu.cn (G. Hu).
[1] These authors contribute equally to this work.

http://dx.doi.org/10.1016/j.redox.2016.08.006

stimulates NLRP3 activation in mouse beta cells [18]. It is now well recognized that the NLRP3 inflammasome is implicated in the pathophysiology of a number of diseases, including depression [19], type 2 diabetes [20], rheumatoid arthritis [21] and Alzheimer's disease [22]. Thus, the functional manipulation of the NLRP3 inflammasome has been thought to be a promising therapeutic strategy for these diseases [23,24]. However, it remains undefined whether the ROS-TXNIP-NLRP3 signal pathway mediates the activation of the NLRP3 inflammasome in astrocytes.

The main source of cellular ROS is mitochondria [25]. Amongst the uncoupling proteins (UCP) identified in the inner membrane of mitochondria, UCP2 is ubiquitously expressed and plays a crucial role in controlling the production of cellular ROS [26]. Recent studies have shown that UCP2 is associated with neurodegenerative diseases such as Parkinson's disease [27], Alzheimer's disease [28] and stroke [29] and its neuroprotective function is likely mediated through restricting the production of ROS and inhibiting inflammation and cell death. Since astrocytes play crucial roles in the development of depression and are the major sites for ROS production as well as innate immune responses [6], we thus hypothesize that astrocytic UCP2 might regulate NLRP3 inflammasome activation and participate in the pathogenesis of depression. In the present study, we prepared chronic mild stress (CMS) model with UCP2 knockout mice so as to investigate the role of UCP2 in depression and cultured primary astrocytes to reveal the underlying mechanism for UCP2-regulated neuroinflammation. It was found that UCP2 knockout exacerbated depressive-like behaviors, impaired neurogenesis, and the loss of astrocytes in CMS-induced model of depression. Furthermore, UCP2 deficiency aggravated NLRP3 inflammasome activation and enhanced ROS-TXNIP-NLRP3 signaling in astrocytes. These findings suggest that UCP2 may be a potential therapeutic target for depression.

2. Materials and methods

2.1. Mice

UCP2$^{-/-}$ mice on a C57/B6 background were originally obtained from Dr. Chenyu Zhang (School of Life Science, Nanjing University, Nanjing, China). UCP2$^{-/-}$ mice and their littermate wild-type controls were bred and maintained in the Animal Resource Centre of the Faculty of Medicine, Nanjing Medical University and age-matched adult male mice (2 month old) used for the experiments. All experiments were carried out in strict accordance with the National Institutes of Health Guide for the Care and Use of Laboratory Animals.

2.2. Chronic mild stress (CMS) procedure

Both genotypic male mice were individually housed and subjected to 5 weeks of stressors, which were mild and unpredictable in nature, duration, and frequency. Stressors included inversion of day/night light cycle, soiled cage bedding, 45° tilted cage, restraint, overnight food and water deprivation, and pairing with another stressed animal. Sucrose preference and body weight of each animal were evaluated weekly until the end of the CMS. The physical state was measured weekly over the entire 5-week stress period using a scale from 1 to 3: a health state was noted 3, a damaged state with piloerection and/or dirty fur noted 1, and an intermediate state noted 2 [30].

2.3. Sucrose preference test

Sucrose preference test was carried out weekly until the end of the CMS. Mice were water deprived for 12 h, and then were allowed to drink from two bottles for 10 h: one contained 1% sucrose solution and the other only tap water. To prevent the possible effect of side-preference in drinking behavior, the positions of the bottles in the cage were switched after the first 5 h. The consumption of tap water, sucrose solution, and total intake of liquids was estimated simultaneously in the control and experimental groups by weighing the bottles. The preference for sucrose was measured as a percentage of the consumed sucrose solution relative to the total amount of liquid intake.

2.4. Tail suspension test

Mice tails were wrapped with tape from the base to the tip, covering about 4/5 of its length and fixed upside down on the hook. The immobility time of each mouse was recorded over a 6-min period. Mice were considered immobile only when they hung passively and completely motionless. The time of immobility of the tail suspended mice during the last 4 min was measured with TailSuspScan™ (Clever Sys Inc., USA).

2.5. Forced swim test

Mice were individually forced to swim in an open cylindrical container (diameter, 15 cm; height, 25 cm), containing 14 cm of water at room temperature (about 22 ± 1 °C) for 6 min. A mouse was judged to be immobile when it floated in an upright position, and made only small movements to keep its head above water. The duration of immobility was recorded during the last 4 min of the 6-min testing period by TailSuspScan™ (Clever Sys Inc., USA). The immobility observed in this test is considered to reflect a state of despair.

2.6. Detection of ROS

In situ detection of ROS was performed as described previously [31]. Dihydroethidium (Molecular Probes) was used to investigate the local *in situ* production of ROS. An intravenous injection of 200 μl dihydroedithium (DHE; stock solution, 100 mg/ml in DMSO, diluted 1:100 with sterile saline before injection) was administered through the caudal vein. Three hours after DHE injection, mice were overdosed with dimethyl ether and transcardially perfused with 4% paraformaldehyde (0.1% glutaraldehyde and 15% picric acid in phosphate buffer). After postfixing overnight in paraformaldehyde without glutaraldehyde, sections at 30 μm were cut through the hippocampus using a Leica freezing microtome. Images were observed and photos were taken under a fluorescent microscope. The intensity of fluorescence was determined by a multimode reader (Vario Skan Flash, 3001, Thermo Scientific) under an emission wavelength at 530 nm and excitation wavelength at 485 nm.

Intracellular ROS was measured with the ROS-specific fluorescent probe 20, 70-dichlorodihydrofluorescein diacetate, acetyl ester (CM-H_2DCFDA; Invitrogen, USA). Astrocytes were incubated with 20 μM H_2DCF-DA for 30 min at 37 °C and washed twice with PBS. The cells then were stained with Hoechst 33342 for 10 min. Images were observed and photos were taken under a confocal microscope (Axiovert LSM510; Carl Zeiss Co.). Fluorescence was measured at $OD_{485–530}$ using a multi-well spectrophotometer.

2.7. Immunohistochemistry and quantification of staining

Following the behavioral tests, the mice were given bromodeoxyuridine (BrdU) intraperitoneally (4 × 50 mg/kg every 2 h, Sigma, US) according to the previous procedures [30]. For analysis of cell proliferation, six mice were killed and transcardially perfused (0.1 M cold phosphate-buffered saline for 5 min followed by

4% cold paraformaldehyde) 24 h after the last BrdU administration. After perfusion, Brain samples were collected and post- fixed in 4% PFA at 4 C overnight. They were transferred to 20% sucrose in phosphate-buffered saline (PBS) overnight and then to 30% sucrose overnight till the brain sunk to the bottom of the tube. Serial sections of the brains were cut (30-μm sections) through each entire hippocampus using a freezing microtome. All sections were collected in six separate series. For immunohistochemistry and immunofluorescence, free-floating sections were placed in a blocking solution consisting of 5% bovine serum albumin (BSA) and 0.3% triton X-100 in 0.01 mol/L PBS for 2 h. For BrdU immunohistochemistry, sections were incubated in anti-mouse BrdU (1:2500; MAB3510, Millipore, USA) overnight at 4 °C h and appropriate anti-mouse secondary antibody for 1 h. Immunostaining was visualized by using substrate-chromogen solution (DAB) for 10 min. For immunofluorescence, sections were incubated with anti-goat doublecortin (DCx, sc-8066, Santa Cruz Biotechnology, USA), or anti- mouse glial fibrillary acidic protein (GFAP, MAB360, Millipore, USA) overnight at 4 °C and the appropriate fluorescent secondary antibody, donkey anti-goat IgG 488 Alexafluore or donkey anti-mouse IgG 488 Alexafluore (1:200; Molecular Probes) for 1 h. Images were observed and photos were taken under a fluorescent microscope. The immunostaining signals were quantitatively analyzed using the Optical Fractionator method with Microbrightfield Stereo-Investigator software (Stereo Investigator software; Microbrightfield). The total number of BrdU- positive cells, DCx- positive cells and GFAP-positive astrocytes in entire extent of hippocampus were counted from six samples per group.

2.8. Culture, transfection and treatment of mouse primary astrocytes

Mouse primary astrocytes were prepared as described previously [27]. Briefly, neonatal mouse (P0–3) were killed by rapid decapitation, the hippocampus was removed and separated from meninges , and tissue was dissociated with 0.25% trypase (Amresco, Solon, OH) at 37 °C and terminated by Dulbecco's modified Eagle's medium (Gibco-BRL, Rockville, MD) supplemented with 10% fetal bovine serum (Sigma, St Louis, MO). After centrifugation at 1500 rpm for 5 min, the cell pellets were resuspended and plated on a poly-lysine–treated flask (Sigma, St Louis, MO). The cultures were maintained at 37 °C in a humidified 5% CO_2–95% air atmosphere. Culture media were changed 24 h later to complete medium and subsequently twice a week. The purity of astrocyte was $>95\%$ as determined with GFAP immunocytochemistry. Before experimental treatments, astrocytic cultures were passaged once. Astrocytes were cultured at a confluency of 70–80% in 24-well dishes and transfected with 1 μg of the full-length human UCP2 cDNA (pcDNA3.1-hUCP2) or the pcDNA3.1 empty vector in OptiMEM (Gibco, USA) using X-tremeGENE HP DNA Transfection Reagent (Roche, Switzerland) for 24 h. For the induction of inflammasome activation, astrocytes were primed with ultrapure lipopolysaccharide (100 ng / ml, Sigma, USA) for 24 h and then pulsed with 250 μg/ml monosodium urate (MSU, Sigma, USA) for 6 h or 5 mM ATP (Sigma, USA) for 30 min. For pharmacological measurements, the caspase-1 inhibitor z-YVAD-zmk (10 μM, Tocris, UK), the ROS inhibitor (2 R,4 R) − 4-amino-pyrrolidine-2, 4-dicarboxylate (APDC, 100 μM, Sigma, USA), or the UCP2 inhibitor genipin (50 μM, Sigma, USA) was added to the cell culture medium 1 h before LPS stimulation. The cell extracts and precipitated supernatants were analyzed by ELISA and immunoblotting.

2.9. Flow cytometry analysis

Mitochondria membrane potential was measured by fluorescence levels upon staining with Mitotracker green (M7514, Invitrogen) and Mitotracker deep red (M22426, Invitrogen) at 50 nM for 30 min at 37 °C and according to the manufacturer's instructions. Mitochondria-associated ROS levels were measured by staining cells with MitoSOX (Invitrogen, USA) at 2.5 μM for 30 min at 37 °C. The cells were then washed with PBS and resuspended in cold PBS containing 1% FBS for flow cytometric analyses.

2.10. Reverse transcription and quantitative real-time PCR

Total RNA was extracted from cultured cells with Trizol reagent (Invitrogen, USA). Reverse transcription PCR was carried out using a TAKARA PrimeScript RT reagent kit and real-time PCR was measured using a QuantiTect SYBR Green PCR kit (Qiagen, Germany) with an ABI 7300 Fast Real-Time PCR System (Applied Biosystems, Foster City, CA). GAPDH was used as an internal control for the real-time PCR amplification. The sequences of primers for real-time PCR analysis are as follows: GAPDH forward primer 5'-CAAAAGGGTCATCTCC-3' and reverse primer 5'-CCCCAGCATCAAAGGTG-3'; UCP2 forward primer 5'-GCTGGTGGTGGTCGGAGAT-3' and reverse primer 5'-TGAAGTGGCAAGGGAGGT-3'; NLRP1 forward primer 5'-CACTGCCCAAGATTGCTACA-3' and reverse primer 5'-CTTCACTCAGCACCAGACCA-3'; NLRP3 forward primer 5'-GTGGTGACCCTCTGTGAGGT-3'and reverse primer 5'-TCTTCCTGGAGCGCTTCTAA-3'; NLRC4 forward primer 5'-CTACATTGATGCTGCCTTGG-3' and reverse primer 5'-ATCCGTCACTGCTCACACAG-3'; AIM2 forward primer 5'-CACCCTCATGGACCTACACTA-3'and reverse primer 5'-CGTTGTTAGTAAATCAGCAGTTCT-3'.

2.11. Elisa

The concentration of IL-1β in the cell culture supernatant and serum was measured by mouse IL-1β ELISA Kit (R&D, USA) according to the manufacturer's instructions.

2.12. Immunoprecipitation

The total cell lysate prepared from astrocytes was incubated with anti-TXNIP (40–3700, Invitrogen) or anti-NLRP3 antibodies (AG-20B-0014-C100, Adipogen) followed by an incubation with protein A/G plus agarose (Santa Cruz Biotechnology, USA) as described previously [18] After washing the beads, the bound proteins were eluted and analyzed by immunoblotting.

2.13. Immunoblotting

Immunoreactive bands were detected by enhanced chemiluminescence (ECL) plus detection reagent (Pierce, Rockford, IL) and analyzed using an Omega 16ic Chemiluminescence Imaging System (Ultra-Lum, CA). The following primary antibodies were used: goat anti-NLRP3 (sc-34410, Santa Cruz Biotechnology, USA), rabbit anti-Caspase-1 (sc-514, Santa Cruz Biotechnology, USA), goat anti-IL-1β (AF-401-NA, R&D, USA), rabbit anti-p65 (Ab536, Abcam, USA), mouse anti-Histone3 (6388, Cell Signaling, USA), mouse anti-TXNIP (K0205–3, MBL, USA) and goat anti-UCP2 (sc-6525, Santa Cruz Biotechnology, USA).

2.14. Statistical analysis

All data are expressed as means ± S.E.M. The differences with different treatments and genotypes were determined by one-way or two-way ANOVA, followed by the Tukey's post hoc test, and were considered as statistically significant at $P<0.05$.

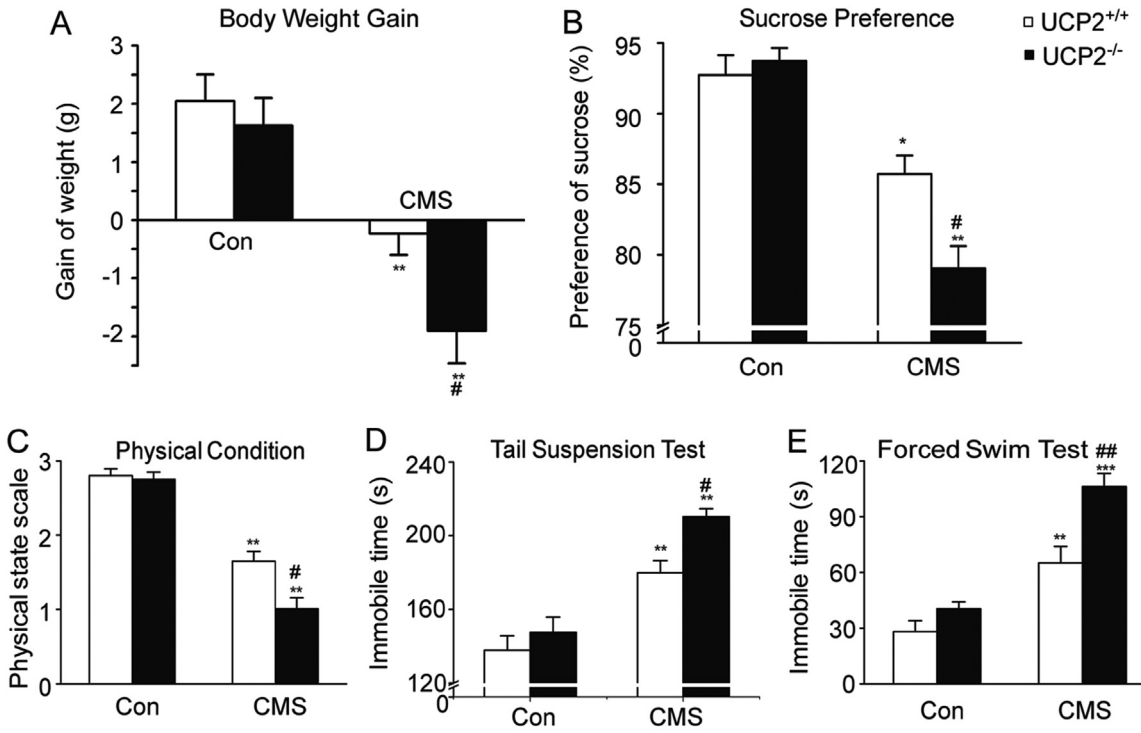

Fig. 1. UCP2 knockout exacerbated CMS-induced depressive responses of mice. (A–E) body weight gain (A), sucrose preference (B), physical states (C), tail suspension test (D) and forced swim test (E) in UCP2$^{+/+}$ and UCP2$^{-/-}$ mice following 5 weeks of CMS. Data are represented as means ± SEM. n = 18–24, $^{*}p < 0.05$, $^{**}p < 0.01$, $^{***}p < 0.001$ vs corresponding control; $^{\#}p < 0.05$, $^{\#\#}p < 0.01$ vs UCP2$^{+/+}$ CMS groups.

3. Results

3.1. UCP2 knockout exacerbates CMS-induced depressive behaviors in mice

To study the role of UCP2 in depression, UCP2 knockout mice were subjected to the CMS procedure and their depressive behaviors analyzed. UCP2$^{-/-}$ mice exhibited a significant decrease in the sucrose preference and in body weight increase compared to UCP2$^{+/+}$ mice after the CMS paradigm (Fig. 1A and B, $P < 0.05$). Although the CMS procedure significantly impaired the physical state in both genotypic mice, the deteriorative effect on the physical state was more remarkable in UCP2$^{-/-}$ mice than that in UCP2$^{+/+}$ mice (Fig. 1C, $P < 0.05$). In both tail suspension and forced swim tests, UCP2 knockout led to a significant increase in the duration of immobility following 5 weeks of CMS (Fig. 1D and E). These data suggest that UCP2 deficiency enhances the progression of depression in adult mice.

3.2. UCP2 knockout aggravates the CMS-induced inhibition of neurogenesis

To study the possible influence of ablating UCP2 on neurogenesis, we compared the cell proliferation of hippocampus in wild-type and UCP2 KO mice. The CMS paradigm significantly reduced the number of BrdU-positive cells by 16% and 27% in the hippocampus of wild-type and UCP2$^{-/-}$ mice, respectively (Fig. 2A and B). Similarly, the CMS significantly decreased the total number of DCx-positive cells in the dentate gyrus in both wild-type and UCP2$^{-/-}$ mice, but the reduction was more severe in UCP2 KO mice than that in UCP2$^{+/+}$ mice (Fig. 2C and D). Furthermore, after the CMS challenge, the number of astrocytes was reduced more potently in UCP2$^{-/-}$ mice than in wild-type mice (Fig. 2E and F, $P < 0.05$). These results demonstrate that UCP2 knockout aggravates the CMS-induced inhibition of neurogenesis and the loss of astrocytes.

3.3. UCP2 deficiency enhances the activation of NLRP3 inflammasome in the hippocampus in vivo and in astrocytes in vitro

As IL-1β is an important inflammatory factor involved in the development of depression [9,32] and its production is tightly controlled by the NLRP3 inflammasome [33] we next determined the effect of UCP2 knockout on the expression of IL-1β and the activation of the NLRP3 inflammasome in the hippocampus. We found that UCP2$^{-/-}$ mice displayed a marked increase in the serum IL-1β compared with UCP2$^{+/+}$ mice after exposure to CMS (Fig. 3A, $P < 0.01$). The CMS procedure also markedly increased the activation of NF-κB and enhanced the expression of NLRP3 in UCP2$^{-/-}$ mice compared with UCP2$^{+/+}$ mice (Fig. 3B and C, $P < 0.05$). Furthermore, the active caspase-1 and the matured IL-1β were significantly increased in the hippocampus of UCP2$^{-/-}$ mice compared to UCP2$^{+/+}$ mice (Fig. 3B and C, $P < 0.05$) following the CMS challenge. These data demonstrate that UCP2 deficiency enhances the CMS-induced the activation of NLRP3 inflammasome in the hippocampus.

Astrocytes are the major sites contributing to the inflammatory responses in the brain and play a crucial role in the pathogenesis of depression [6]. We found that both UCP2 and NLRP3 are highly expressed in astrocytes (Fig. 3D-F). Therefore, we then sought to study the regulation of NLRP3 inflammasome by UCP2 in astrocytes. Astrocytes were isolated from wild-type and UCP2 knockout mice and treated with the NLRP3 inflammasome activators ATP and MSU. Similar to the results obtained in the hippocampus, the enhancements in the activation of NF-κB and caspase-1 and the expression of NLRP3 and IL-1β after the treatment with ATP and MSU were much more potent in astrocytes prepared from UCP2$^{-/-}$ KO mice than those from UCP2$^{+/+}$ mice ($P < 0.05$) (Fig. 3G and H). Consistently, the treatment with the UCP2 pharmacological inhibitor genipin (50 μM) facilitated the activation of caspase-1 and expression of IL-1β in UCP2$^{+/+}$ astrocytes stimulated with LPS plus MSU, but not in UCP2$^{-/-}$ astrocytes (Fig. 3I and J, $P < 0.05$). Furthermore, treatment with the caspase-1 inhibitor z-YVAD-fmk

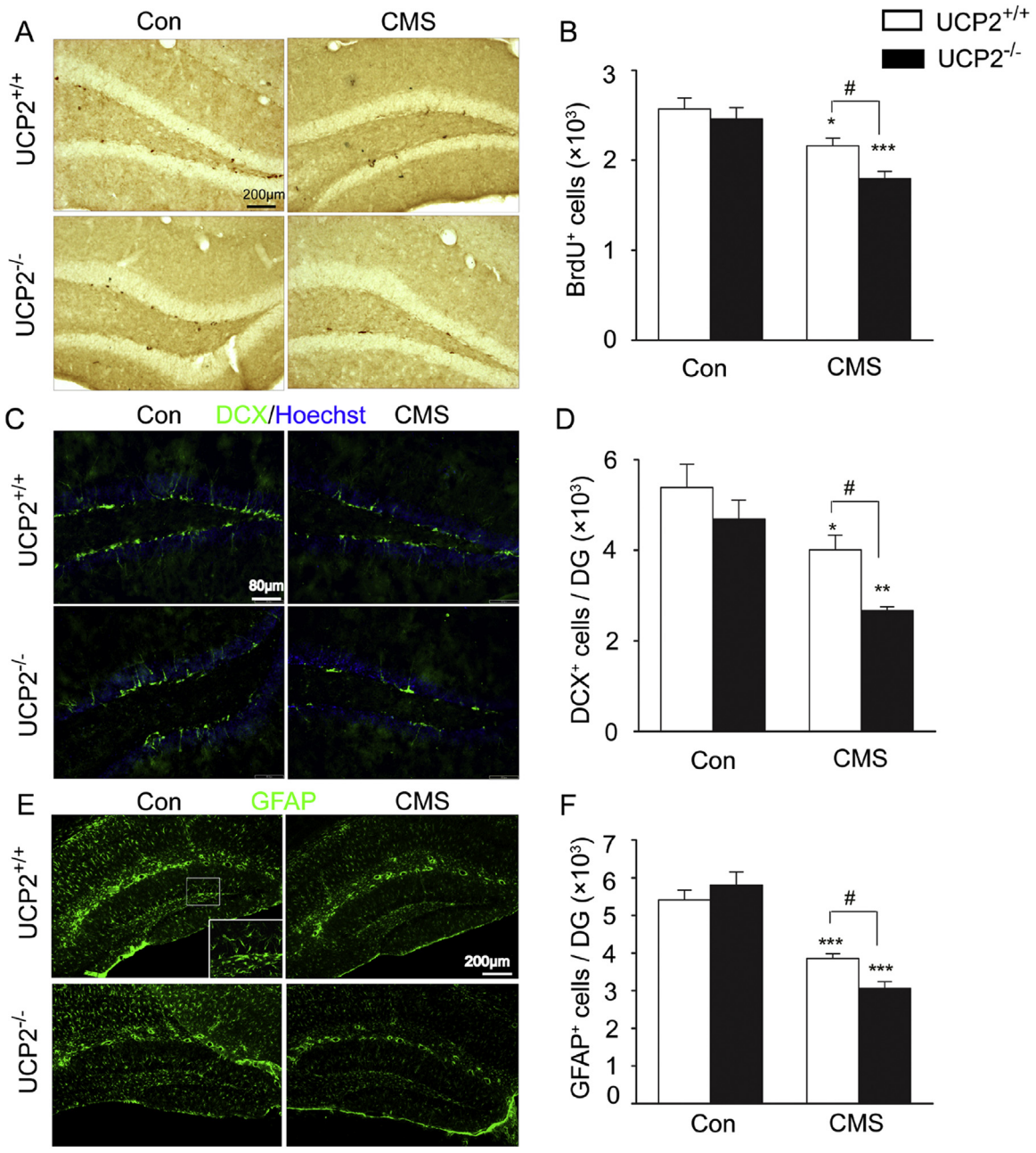

Fig. 2. UCP2 deletion aggravated CMS-induced inhibition of neurogenesis and the loss of astrocytes in mice. (A-F) Immunohistochemical staining and stereological counts of $BrdU^+$ (A–B), DCx^+ (C-D) and $GFAP^+$ (E–F) cells in the s hippocampus of $UCP2^{+/+}$ and $UCP2^{-/-}$ mice following 5 weeks of CMS. Data are represented as means ± SEM. n = 6, $^{*}p < 0.05$, $^{**}p < 0.01$, $^{***}p < 0.001$ vs corresponding control; $^{\#}p < 0.05$ vs $UCP2^{+/+}$ CMS groups.

(10 μM) suppressed the enhanced IL-1β secretion in $UCP2^{-/-}$ astrocytes, which confirmed that the greater abundance of IL-1β was the consequence of more caspase-1 activity (Fig. 3K). These results demonstrate that, similar to the hippocampus, UCP2 deficiency also promotes the activation of NLRP3 inflammasome in astrocytes.

3.4. The ROS-TXNIP-NLRP3 signaling pathway mediates the NLRP3 inflammasome activation in UCP2 knockout astrocytes

Our preceding data have strongly demonstrated that UCP2 is a negative regulator of the NLRP3 inflammasome. To dissect the underlying molecular mechanisms, we first measured the functional mitochondrial pool in wild-type and UCP2 KO astrocytes using mitochondria-specific labels which are able to distinguish the respiring (Mitotracker deep red) and total (Mitotracker green) mitochondria. Treatments with LPS and MSU produced a greater loss of mitochondrial membrane potential and increase in mitochondrial volume in UCP2 KO than in wild-types (Fig. 4A–C, $P < 0.05$). As mitochondria are the main source of cellular ROS, we then determined the effect of UCP2 KO on the production of ROS in the hippocampus and in astrocytes. The CMS procedure markedly augmented the ROS production in the hippocampus and $UCP2^{-/-}$ mice displayed a higher level of ROS compared to WT mice as evaluated by the fluorescence of DHE (Fig. 4D and E, $P < 0.05$). Similarly, UCP2 KO astrocytes generated more mitochondrial ROS as detected by the fluorescence of MitoSOX (Fig. 4F, $P < 0.05$) and intracellular ROS as measured by the fluorescence of CM-H_2DCFDA (Fig. 4G and H, $P < 0.05$) than wild-type astrocytes.

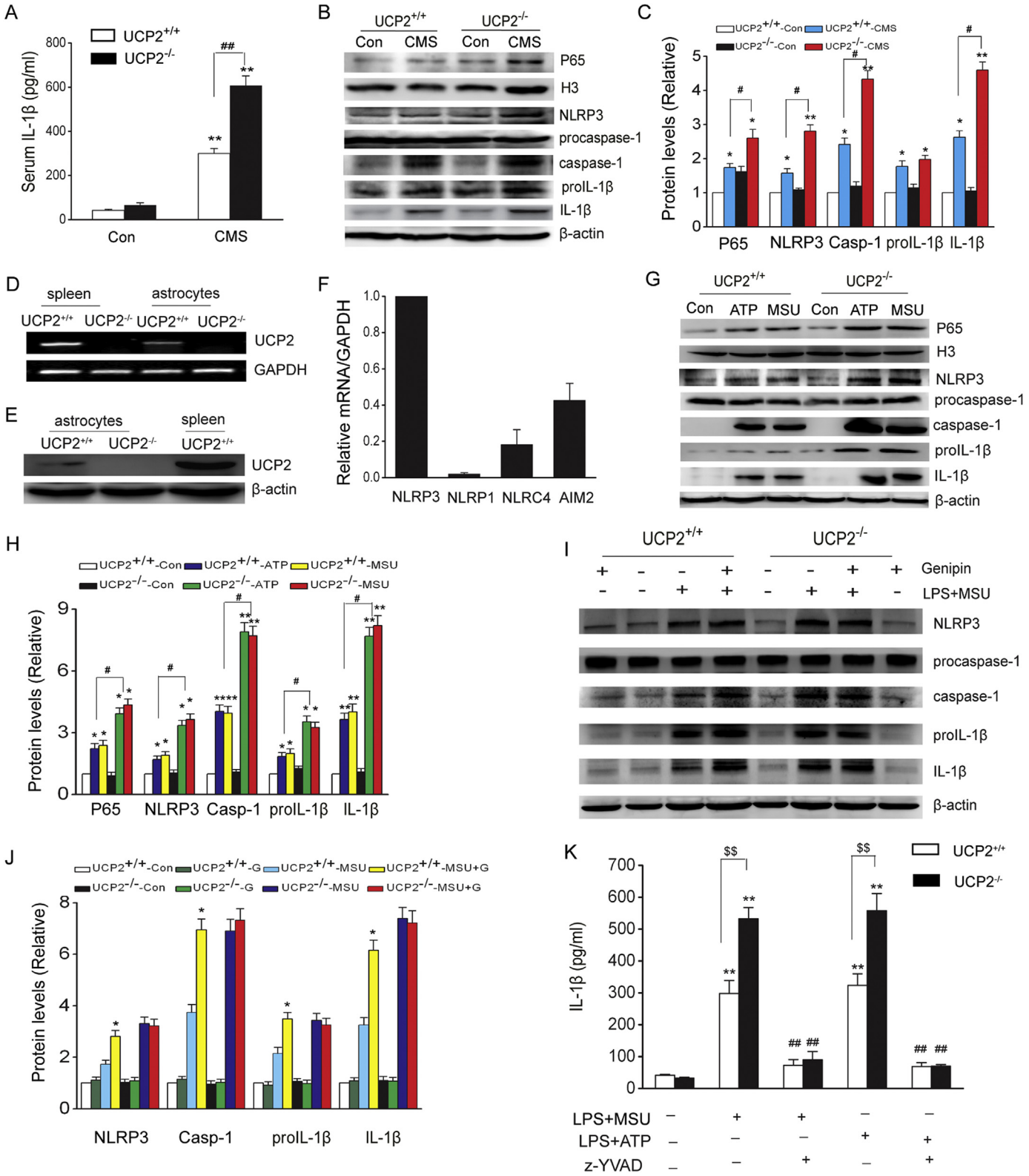

Fig. 3. UCP2 deficiency enhanced the activation of NLRP3 inflammasome in hippocampus and in mouse astrocytes. (A) ELISA of serum Il-1β (n=10/group). (B-C) Representative Immunoblot (B) and quantitative (C) analysis of nucelus p65, NLRP3, procaspase-1, caspase-1, proIL-1β, and Il-1β in the hippocampus of $UCP2^{+/+}$ and $UCP2^{-/-}$ mice (n=4/group). (D-E) mRNA (D) and protein levels of UCP2 (E) in astrocyte and spleen (positive control) of $UCP2^{+/+}$ and $UCP2^{-/-}$ mice. (F) Real-time PCR analysis of mRNA levels of NLRP3, NLRP1, NLRC4 and AIM2 in astrocytes. (G–H) Representative Immunoblot (G) and quantitative (H) analysis of nucelus p65, NLRP3, procaspase-1, caspase-1, proIL-1β, and Il-1β in astrocytes from $UCP2^{+/+}$ and $UCP2^{-/-}$ mice. (I–J) Representative Immunoblot (I) and quantitative analysis (J) of NLRP3, procaspase-1, caspase-1, proIL-1β, and Il-1β in lysates and supernatants of $UCP2^{+/+}$ and $UCP2^{-/-}$ astrocytes incubated for 1 h with genipin (G, 50 μM), followed by stimulation with LPS+MSU. (K) ELISA of Il-1β secretion by $UCP2^{+/+}$ and $UCP2^{-/-}$ astrocytes incubated for 1 h with z-YVAD-fmk (z-YVAD; 10 μM), followed by stimulation with LPS+ATP or LPS+MSU. Data are represented as means ± SEM from four independent experiments. $^{*}p<0.05$, $^{**}p<0.01$ vs corresponding control; $^{\#}p<0.05$, $^{\#\#}p<0.01$.

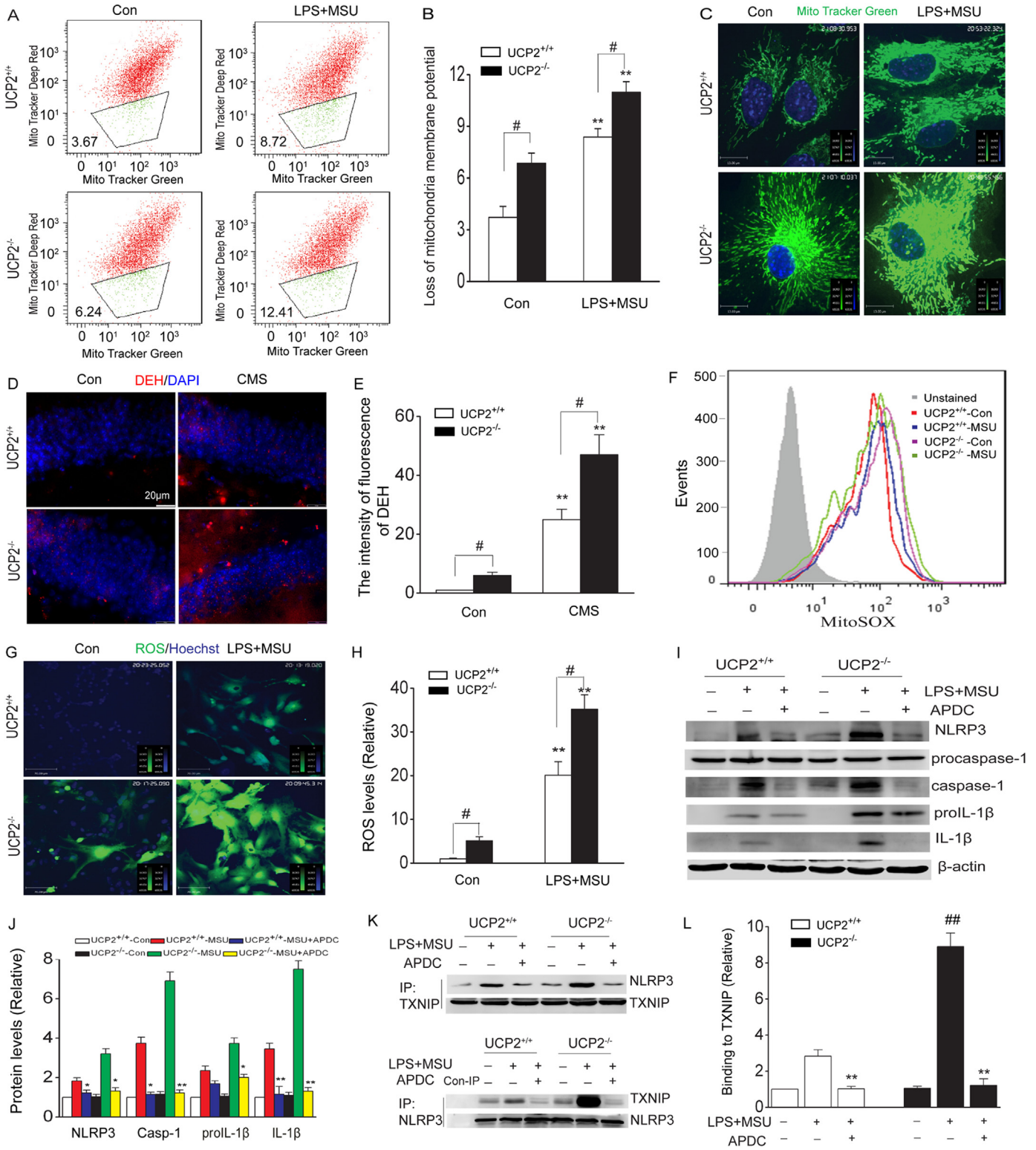

Fig. 4. ROS-TXNIP-NLRP3 signaling pathway contributed to the enhancement of NLRP3 inflammasome activation in UCP2 knockout astrocytes. (A–B) Astrocytes were stimulated with LPS+MSU for 6 h and then stained with Mitotrackergreen and Mitotracker deep red for 30 min and analyzed by flow cytometry (A). B, Quantification of the mitochondrial membrane potential. (C) Confocal microscopy of morphological changes in mitochondria monitored by staining with Mitotrackergreen. (D-E) UCP2 knockout increased ROS production in vivo. D, Photos were taken at $\times 600$ magnification. Red color represents DEH and blue color represents nucleus. Scale bar=22 μm. E, Quantification of the fluorescence intensity of the DEH staining to assess ROS level in vivo (n=6/group). (F-H) Astrocytes were stimulated with LPS+MSU for 6 h and then stained with MitoSOX (F) or CM-H_2DCFDA labeling (G–H) for 30 min and analyzed by flow cytometry or confocal microscope. (I–J) Representative Immunoblot (I) and quantitative analysis (J) of NLRP3, procaspase-1, caspase-1, proIL-1β, and Il-1β in the presence of ROS inhibitor (APDC, 100 μM). (K–L) Immunoprecipitation and immunoblot analysis of the interaction of TXNIP with NLRP3 in the presence of ROS inhibitor (APDC, 100 μM). Data are represented as means ± SEM from four independent experiments. $^{**}p < 0.01$ vs corresponding control; $^{\#}p < 0.05$, $^{\#\#}p < 0.01$.

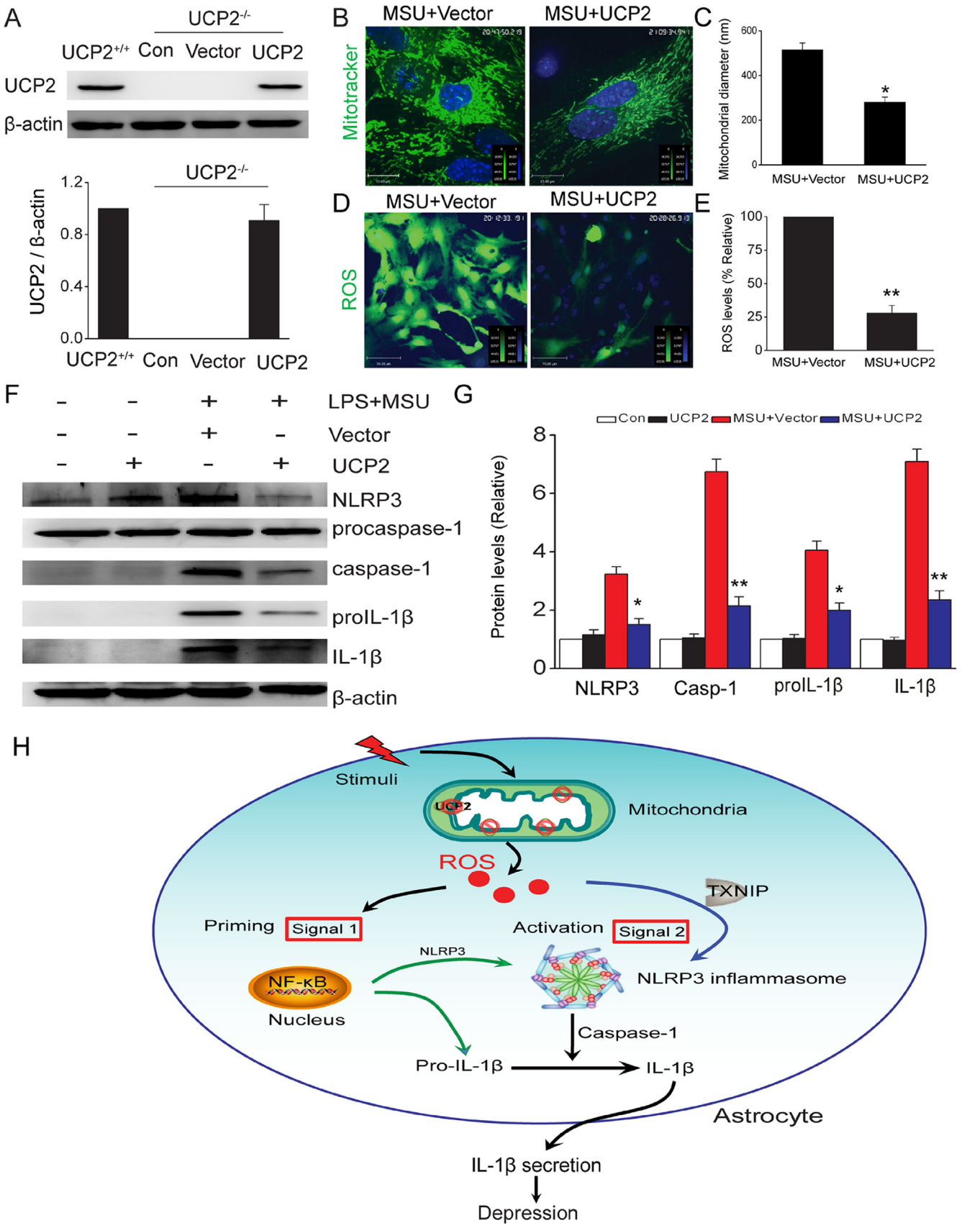

Fig. 5. Rescue of UCP2 inhibited ROS production and NLRP3 inflammasome activation in mouse astrocytes. UCP2$^{-/-}$ astrocytes were transfected with either full-length human UCP2 cDNA plasmid (UCP2) or pcDNA3.1 empty vector (vector) for 24 h, and then stimulated with LPS+MSU. (A) The expression of UCP2 in UCP2$^{+/+}$ astrocytes and UCP2$^{-/-}$ astrocytes transfected with either full-length human UCP2 cDNA plasmid (UCP2) or pcDNA3.1 empty vector (vector) for 24 h. (B-C) Confocal microscopy of morphological changes in mitochondria monitored by staining with Mitotrackergreen (B) and quantification of mitochondrial diameter (C). (D-E) Rescue of UCP2 inhibited ROS production in astrocytes. D, Photos were taken by confocal. E, Quantification of the fluorescence intensity of the CM-H2DCFDA staining to assess intracellular ROS level. (F-G) Representative Immunoblot (F) and quantitative analysis (G) of NLRP3, procaspase-1, caspase-1, proIL-1β, and Il-1β in lysates and supernatants of astrocytes. (H) Schematic layout of showing UCP2 knockout aggravates major depressive disorder via enhancing NLRP3 inflammasome activation in mouse astrocytes. Data are represented as means ± SEM from four independent experiments. $^{*}p < 0.05$, $^{**}p < 0.01$ vs MSU+vector group.

To determine whether UCP2 knockout-induced ROS production contributed to the activation of NLRP3 inflammasome, the primary cultures of astrocytes were treated with the ROS inhibitor APDC. The APDC treatment significantly abrogated the increase in IL-1β secretion and caspase-1 activation in UCP2 KO astrocytes treated with LPS and MSU (Fig. 4I and J). It has been demonstrated that TXNIP binds to and activates NLRP3 in ROS dependent manner [18]. We then determined if UCP2 KO could alter the interaction between TXNIP and NLRP3. As shown in Fig. 4K and L, UCP2 KO resulted in a significant increase in the TXNIP-NLRP3 association, and this effect was abolished by APDC treatment. These data suggest that the function of UCP2 in regulating the NLRP3 inflammasome activation is likely mediated through the ROS-TXNIP-NLRP3 signaling pathway in astrocytes.

3.5. Transient expression of UCP2 rescues the mitochondrial injury, ROS production and the NLRP3 inflammasome activation in astrocytes lacking UCP2

To further define the role of UCP2 in depression and the NLRP3 inflammasome activation as observed in the UCP2 KO mice, we determined if transiently expressing UCP2 could reverse the deleterious effects of ablating UCP2 on the mitochondrial function, ROS production and the NLRP3 inflammasome activation in astrocytes. UCP2 was transiently expressed in astrocytes isolated from UCP2 KO mice at a level similar to the expression of endogenous UCP2 (Fig. 5A). Increased UCP2 expression dramatically alleviated the swollen mitochondria (Fig. 5B and C) and reduced ROS production in UCP2 KO astrocytes (Fig. 5D and E). Expression of UCP2 also attenuated NLRP3 expression, caspase-1 activation and IL-1β secretion in response to LPS and MSU stimulation (Fig. 5F and G). These data indicate the re-expression of UCP2 could protect astrocytes from the damage.

4. Discussion

The most important finding presented here is that UCP2 is a crucial regulator of the NLRP3 inflammasome in astrocytes. Activation of the NLRP3 inflammasome requires two signals [34]. The first signal is provided by microbial or endogenous molecules that activate NF-κB to induce NLRP3 expression, which is a prerequisite for inflammasome activation [15,35]. The second signal directly activates the NLRP3 inflammasome to induce the activation of caspase-1, leading to the maturation of the proinflammatory cytokines IL-1β and IL-18 [36]. In the present study, we found that the activation of NF-κB and the expression of NLRP3 were significantly higher in UCP2$^{-/-}$ mice than UCP2$^{+/+}$ mice after the exposure to CMS. We also observed that, compared with UCP2$^{+/+}$ mice, UCP2$^{-/-}$ mice displayed a significant increase in the activation of caspase-1 and the maturation of IL-1β following CMS. These data indicate that UCP2 deficiency enhances both the priming and the activation of the NLRP3 inflammasome.

Our study further reveals the molecular mechanism underlying the function of UCP2 in regulating the activation of NLRP3 inflammasome in astrocyets. The production of ROS is believed to be a common activator of the NLRP3 inflammasome [37]. However, the role of physical association of NLRP3 with TXNIP in the ROS-dependent activation of NLRP3 inflammasome has been contradictory [38,39]. In this study, we found that UCP2 knockout not only increased the ROS production but also promoted the TXNIP-NLRP3 association in mouse astrocytes. Furthermore, treatment with the ROS inhibitor APDC almost abolished the association of TXNIP with NLRP3 and the activation of NLRP3 inflammasome in UCP2 knockout astrocytes. These data demonstrate that the function of UCP2 in regulating the activation of NLRP3 inflammasome is mediated through controlling the production of ROS and the association of NLRP3 with TXNIP in astrocytes. This mechanism is also consistent with other reports demonstrating the role of ROS and the TXNIP-NLRP3 interaction in the activation of the NLRP3 inflammasomes in other cell types including primary rat hepatocytes , endothelial cells [40] and mouse beta cells [18]. Taken together, these findings indicate that the ROS-TXNIP-NLRP3 signal pathway contributes to the modulation of the NLRP3 inflammasome activation by UCP2.

Another important finding described here is that we provide strong evidence further indicating that UCP2 plays an important role in the pathogenesis of depression. We used UCP2$^{-/-}$ mice to establish a CMS-induced anhedonia model of depression and found that UCP2$^{-/-}$ mice displayed the lower sucrose preference (anhedonia) and bodyweight. UCP2 knockout mice also had remarkable deterioration of the physical state and a significant increase in the duration of immobility. These data, together with our previous report [41], indicate that UCP2 knockout aggravated depressive-like behaviors. Consistent with the observed deleterious effects on the behaviors, we found that UCP2 knockout reduced the ability of neurogenesis in the hippocampus and enhanced the loss of astrocytes. These data suggest that both the impaired neurogenesis and the reduced astrocytes may contribute to the depressive behaviors observed in UCP2 KO mice.

Growing evidence indicates that astrocytes cannot be just considered as passive supportive cells deputed to preserve neuronal activity and survival, but rather they are involved in a striking number of active functions that are critical to the performance of the central nervous system [42]. Recently, animal studies and postmortem brain analyses of patients with depression implicated glial dysfunction in MDD pathophysiology [43,44]. Astrocytes-mediated inflammation plays an important role in the pathogenesis of depression [45] and neurodegenerative diseases such as Alzheimer Disease [46], Parkinson Disease [27] and stroke [47]. UCP2 knockout enhanced the activation of NLRP3 inflammasome and increased the production of IL-1β in astrocytes, indicating that astrocytic UCP2 is involved in the development of the NLRP3 inflammasome-driven inflammatory diseases, including depression.

In conclusion, our study demonstrates that UCP2 knockout aggravates depressive-like behaviors, impairs neurogenesis, and promotes the loss of astrocytes in CMS-induced model of depression. Furthermore, UCP2 deficiency exacerbates NLRP3 inflammasome activation and enhances ROS-TXNIP-NLRP3 signaling in astrocytes (Fig. 5H). Collectively, our findings reveal that UCP2 negatively regulates inflammation responses in astrocytes and plays an important role in the pathogenesis of depression and that UCP2 may be a promising therapeutic target for depression.

Conflicts of interest

The authors declare no conflict of interest.

Acknowledgements

This work was supported by the Grant from the National Natural Science Foundation of China (Nos. 81630099, 81473196 and 81573403). We would like to thank Dr. Chenyu Zhang (School of Life Sciences, Nanjing University) for providing UCP2 knockout mice.

References

[1] N. Cai, T.B. Bigdeli, W. Kretzschmar, Y. Li, J. Liang, L. Song, et al., Sparse whole-genome sequencing identifies two loci for major depressive disorder, Nature

523 (2015) 588–591.
[2] M.H. Kokacya, B. Bahceci, I. Bahceci, A.R. Dilek, R. Dokuyucu, Prolidase activity and oxidative stress in patients with major depressive disorder, Psychiatr. Danub 26 (2014) 314–318.
[3] E.H. Tobe, Mitochondrial dysfunction, oxidative stress, and major depressive disorder, Neuropsychiatr. Dis. Treat. 9 (2013) 567–573.
[4] H. Wang, J. Warner-Schmidt, S. Varela, G. Enikolopov, P. Greengard, M. Flajolet, Norbin ablation results in defective adult hippocampal neurogenesis and depressive-like behavior in mice, Proc. Natl. Acad. Sci. USA 112 (2015) 9745–9750.
[5] G.M. Slavich, M.R. Irwin, From stress to inflammation and major depressive disorder: a social signal transduction theory of depression, Psychol. Bull. 140 (2014) 774–815.
[6] S. Hashioka, T. Miyaoka, R. Wake, M. Furuya, J. Horiguchi, Glia: an important target for anti-inflammatory and antidepressant activity, Curr. Drug Targets 14 (2013) 1322–1328.
[7] X.H. Dong, X.C. Zhen, Glial pathology in bipolar disorder: potential therapeutic implications, CNS Neurosci. Ther. 21 (2015) 393–397.
[8] G.Z. Reus, G.R. Fries, L. Stertz, M. Badawy, I.C. Passos, T. Barichello, et al., The role of inflammation and microglial activation in the pathophysiology of psychiatric disorders, Neuroscience 300 (2015) 141–154.
[9] G.J. Norman, K. Karelina, N. Zhang, J.C. Walton, J.S. Morris, A.C. Devries, Stress and IL-1beta contribute to the development of depressive-like behavior following peripheral nerve injury, Mol. Psychiatry 15 (2010) 404–414.
[10] J.P. Konsman, J. Veeneman, C. Combe, S. Poole, G.N. Luheshi, R. Dantzer, Central nervous action of interleukin-1 mediates activation of limbic structures and behavioural depression in response to peripheral administration of bacterial lipopolysaccharide, Eur. J. Neurosci. 28 (2008) 2499–2510.
[11] J.W. Koo, R.S. Duman, Interleukin-1 receptor null mutant mice show decreased anxiety-like behavior and enhanced fear memory, Neurosci. Lett. 456 (2009) 39–43.
[12] C.D. Rethorst, M.S. Toups, T.L. Greer, P.A. Nakonezny, T.J. Carmody, B. D. Grannemann, et al., Pro-inflammatory cytokines as predictors of antidepressant effects of exercise in major depressive disorder, Mol. Psychiatry 18 (2013) 1119–1124.
[13] L. Broderick, D. De Nardo, B.S. Franklin, H.M. Hoffman, E. Latz, The inflammasomes and autoinflammatory syndromes, Annu Rev. Pathol. 10 (2015) 395–424.
[14] A. Abderrazak, T. Syrovets, D. Couchie, K. El Hadri, B. Friguet, T. Simmet, et al., NLRP3 inflammasome: from a danger signal sensor to a regulatory node of oxidative stress and inflammatory diseases, Redox Biol. 4 (2015) 296–307.
[15] H.C. Guo, Y. Jin, X.Y. Zhi, D. Yan, S.Q. Sun, NLRP3 inflammasome activation by viroporins of animal viruses, Viruses 7 (2015) 3380–3391.
[16] T. Luna-Gomes, P.T. Santana, R. Coutinho-Silva, Silica-induced inflammasome activation in macrophages: role of ATP and P2X7 receptor, Immunobiology 220 (2015) 1101–1106.
[17] R. Suarez, N. Buelvas, Inflammasome: activation mechanisms, Investig. Clin. 56 (2015) 74–99.
[18] R. Zhou, A. Tardivel, B. Thorens, I. Choi, J. Tschopp, Thioredoxin-interacting protein links oxidative stress to inflammasome activation, Nat. Immunol. 11 (2010) 136–140.
[19] E. Alcocer-Gomez, C. Ulecia-Moron, F. Marin-Aguilar, T. Rybkina, N. Casas-Barquero, J. Ruiz-Cabello, et al., Stress-Induced Depressive Behaviors Require a Functional NLRP3 Inflammasome, Mol. Neurobiol. (2015), Sep 11. [Epub ahead of print].
[20] H.J. Lee, Y.S. Hong, W. Jun, S.J. Yang, Nicotinamide riboside ameliorates hepatic metaflammation by modulating NLRP3 inflammasome in a rodent model of Type 2 diabetes, J. Med. Food 18 (2015) 1207–1213.
[21] P. Ruscitti, P. Cipriani, P. Di Benedetto, V. Liakouli, O. Berardicurti, F. Carubbi, et al., Monocytes from patients with rheumatoid arthritis and type 2 diabetes mellitus display an increased production of interleukin (IL)-1beta via the nucleotide-binding domain and leucine-rich repeat containing family pyrin 3 (NLRP3)-inflammasome activation: a possible implication for therapeutic decision in these patients, Clin. Exp. Immunol. 182 (2015) 35–44.
[22] M.T. Heneka, M.P. Kummer, A. Stutz, A. Delekate, S. Schwartz, A. Vieira-Saecker, et al., NLRP3 is activated in Alzheimer's disease and contributes to pathology in APP/PS1 mice, Nature 493 (2013) 674–678.
[23] R.C. Coll, A.A. Robertson, J.J. Chae, S.C. Higgins, R. Munoz-Planillo, M.C. Inserra, et al., A small-molecule inhibitor of the NLRP3 inflammasome for the treatment of inflammatory diseases, Nat. Med. 21 (2015) 248–255.
[24] E. Ozaki, M. Campbell, S.L. Doyle, Targeting the NLRP3 inflammasome in chronic inflammatory diseases: current perspectives, J. Inflamm. Res. 8 (2015) 15–27.
[25] P.H. Willems, R. Rossignol, C.E. Dieteren, M.P. Murphy, W.J. Koopman, Redox homeostasis and mitochondrial dynamics, Cell Metab. 22 (2015) 207–218.
[26] C. Toda, S. Diano, Mitochondrial UCP2 in the central regulation of metabolism, Best Pract. Res Clin. Endocrinol. Metab. 28 (2014) 757–764.
[27] M. Lu, X.L. Sun, C. Qiao, Y. Liu, J.H. Ding, G. Hu, Uncoupling protein 2 deficiency aggravates astrocytic endoplasmic reticulum stress and nod-like receptor protein 3 inflammasome activation, Neurobiol. Aging 35 (2014) 421–430.
[28] Z. Wu, Y. Zhao, B. Zhao, Superoxide anion, uncoupling proteins and Alzheimer's disease, J. Clin. Biochem. Nutr. 46 (2010) 187–194.
[29] B.A. Haines, S.L. Mehta, S.M. Pratt, C.H. Warden, P.A. Li, Deletion of mitochondrial uncoupling protein-2 increases ischemic brain damage after transient focal ischemia by altering gene expression patterns and enhancing inflammatory cytokines, J. Cereb. Blood Flow Metab. 30 (2010) 1825–1833.
[30] H. Kong, L.L. Sha, Y. Fan, M. Xiao, J.H. Ding, J. Wu, et al., Requirement of AQP4 for antidepressive efficiency of fluoxetine: implication in adult hippocampal neurogenesis, Neuropsychopharmacology 34 (2009) 1263–1276.
[31] M. Lu, F.F. Zhao, J.J. Tang, C.J. Su, Y. Fan, J.H. Ding, et al., The neuroprotection of hydrogen sulfide against MPTP-induced dopaminergic neuron degeneration involves uncoupling protein 2 rather than ATP-sensitive potassium channels, Antioxid. Redox Signal 17 (2012) 849–859.
[32] M. Maes, C. Song, R. Yirmiya, Targeting IL-1 in depression, Exp. Opin. Ther. Targets 16 (2012) 1097–1112.
[33] H. Wen, E.A. Miao, J.P. Ting, Mechanisms of NOD-like receptor-associated inflammasome activation, Immunity 39 (2013) 432–441.
[34] J. Gao, R.T. Liu, S. Cao, J.Z. Cui, A. Wang, E. To, et al., NLRP3 inflammasome: activation and regulation in age-related macular degeneration, Mediat. Inflamm. (2015) 690243.
[35] J.J. Kim, E.K. Jo, NLRP3 inflammasome and host protection against bacterial infection, J. Korean Med. Sci. 28 (2013) 1415–1423.
[36] B. Sun, X. Wang, Z. Ji, R. Li, T. Xia, NLRP3 inflammasome activation induced by engineered nanomaterials, Small 9 (2013) 1595–1607.
[37] M.E. Heid, P.A. Keyel, C. Kamga, S. Shiva, S.C. Watkins, R.D. Salter, Mitochondrial reactive oxygen species induces NLRP3-dependent lysosomal damage and inflammasome activation, J. Immunol. 191 (2013) 5230–5238.
[38] Y. Liu, K. Lian, L. Zhang, R. Wang, F. Yi, C. Gao, et al., TXNIP mediates NLRP3 inflammasome activation in cardiac microvascular endothelial cells as a novel mechanism in myocardial ischemia/reperfusion injury, Basic Res. Cardiol. 109 (2014) 415.
[39] S.L. Masters, A. Dunne, S.L. Subramanian, R.L. Hull, G.M. Tannahill, F.A. Sharp, et al., Activation of the NLRP3 inflammasome by islet amyloid polypeptide provides a mechanism for enhanced IL-1beta in type 2 diabetes, Nat. Immunol. 11 (2010) 897–904.
[40] I.N. Mohamed, S.S. Hafez, A. Fairaq, A. Ergul, J.D. Imig, A.B. El-Remessy, Thioredoxin-interacting protein is required for endothelial NLRP3 inflammasome activation and cell death in a rat model of high-fat diet, Diabetologia 57 (2014) 413–423.
[41] X.L. Sun, Y. Liu, T. Dai, J.H. Ding, G. Hu, Uncoupling protein 2 knockout exacerbates depression-like behaviors in mice via enhancing inflammatory response, Neuroscience 192 (2011) 507–514.
[42] V. Rothhammer, F.J. Quintana, Control of autoimmune CNS inflammation by astrocytes, Semin Immunopathol. 37 (2015) 625–638.
[43] G. Rajkowska, C.A. Stockmeier, Astrocyte pathology in major depressive disorder: insights from human postmortem brain tissue, Curr. Drug Targets 14 (2013) 1225–1236.
[44] M. Banasr, G.M. Chowdhury, R. Terwilliger, S.S. Newton, R.S. Duman, K. L. Behar, et al., Glial pathology in an animal model of depression: reversal of stress-induced cellular, metabolic and behavioral deficits by the glutamate-modulating drug riluzole, Mol. Psychiatry 15 (2010) 501–511.
[45] W.K. Jo, Y. Zhang, H.M. Emrich, D.E. Dietrich, Glia in the cytokine-mediated onset of depression: fine tuning the immune response, Front. Cell Neurosci. 9 (2015) 268.
[46] E.C. Phillips, C.L. Croft, K. Kurbatskaya, M.J. O'Neill, M.L. Hutton, D.P. Hanger, et al., Astrocytes and neuroinflammation in Alzheimer's disease, Biochem. Soc. Trans. 42 (2014) 1321–1325.
[47] M. Gliem, K. Krammes, L. Liaw, N. van Rooijen, H.P. Hartung, S. Jander, Macrophage-derived osteopontin induces reactive astrocyte polarization and promotes re-establishment of the blood brain barrier after ischemic stroke, Glia 63 (2015) 2198–2207.